Journal Name

ARTICLE

Iron(II) complexes of tris(2-pyridylmethyl)amine (TPMA) and neutral bidentate ligands showing thermal- and photo-induced Spin Crossover

Received 00th January 20xx,
Accepted 00th January 20xx

DOI: 10.1039/x0xx00000x

www.rsc.org/

Víctor García-López,[a] João C. Waerenborgh,[b] Bruno J. C. Vieira,[b] Miguel Clemente-León,*[a] and Eugenio Coronado*[a]

Three new mononuclear Fe(II) complexes have been prepared and characterized by the combination of tetradentate tris(2-pyridylmethyl)amine (TPMA) with three neutral bidentate ligands, such as ethylenediamine (en), 1,2-diaminopropane (pn) and 2-picolylamine (2-pic), in compounds $[Fe^{II}(TPMA)(en)](ClO_4)_2$ **(1),** $[Fe^{II}(TPMA)(2\text{-pic})](ClO_4)_2$ **(2)** and $[Fe^{II}(TPMA)(pn)](ClO_4)_2$ **(3)**. Structural and magnetic characterization demonstrates that the three compounds present a complete SCO behavior. The absence of strong intermolecular interactions and solvent molecules leads to reversible and gradual spin transitions. The different ligands allow tuning $T_{1/2}$ from 130 K (**2**) to 325 K (**3**). The compound with the lowest $T_{1/2}$ (**2**) shows LIESST effect with a T_{LIESST} of 43 K. Interestingly, the use of these relatively small bidentate ligands leads to the crystallization in non-centrosymmetric space groups in contrast with previous works using other bidentate ligands.

Introduction

Spin-crossover (SCO) complexes can be reversibly switched between two distinct spin states, low-spin (LS) and high-spin (HS) through a variety of external stimuli (temperature, pressure or electromagnetic radiation).[1] Upon spin-state switching, significant changes in structure, color and magnetism occur. As a result of this, SCO materials have been proposed for many applications, such as sensors or memory and spintronic devices.[2,3]

Tetradentate Tris(2-pyridylmethyl)amine (TPMA) ligand also known as TPA has shown to be effective for achieving temperature and light driven SCO in a great number of iron(II) complexes. Thus, coordination of the two free coordination sites in cis configuration by two charged ligands such as NCS^-, $NCSe^-$ or $NCBH_3^-$ have afforded neutral mononuclear SCO complexes,[4] while the use of neutral bidentate N-alkylated 2,2'-bisimidazole derivatives has led to charged mononuclear SCO complexes,[5] which could be combined with a $TCNQ^{\bullet-}$ radical anion for the preparation of multifunctional compounds with coexistence of conductivity and SCO.[6] In addition to this, the coordination of potentially bridging ligands has allowed the design of polynuclear SCO derivatives, such as dimers[7] or tetramers.[8]

In spite of the wide use of this ligand, the preparation of mononuclear charged complexes combining TPMA with a neutral bidentate ligand has remained almost unexplored.[5] In this work, we have tempted the preparation of charged iron(II) SCO complexes combining TPMA with three neutral bidentate ligands, such as ethylenediamine (en), 1,2-diaminopropane (pn) and 2-picolylamine (2-pic) (Scheme 1), which generate different crystal fields around octahedral Fe(II). These cationic complexes could be used for the synthesis of new multifunctional compounds by combination with anionic functional units.

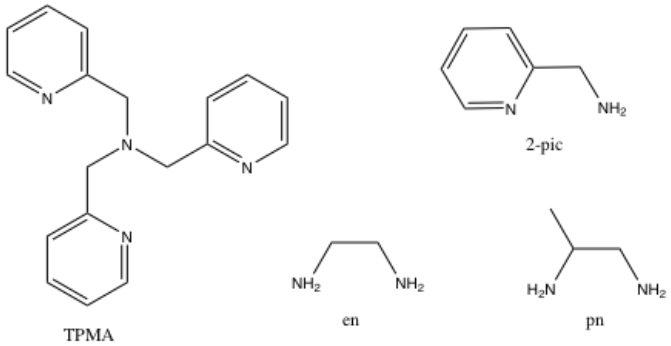

Scheme 1 Ligands used in this work: TPMA = tris(2-pyridylmethyl)amine, en = ethylenediamine, pn = 1,2-diaminopropane and 2-pic = 2-picolylamine.

Results and discussion

Synthesis.

[a] Instituto de Ciencia Molecular (ICMol), Universidad de Valencia, C/ Catedrático José Beltrán 2, 46980 Paterna, Spain. Fax: 34 963543273; Tel: 34 963544419; E-mail: miguel.clemente@uv.es.
[b] Centro de Ciências e Tecnologias Nucleares, Instituto Superior Técnico, Universidade de Lisboa, 2695-066 Bobadela LRS, Portugal

†Electronic Supplementary Information (ESI) available: Electronic supplementary information (ESI) available: ESI contains powder X ray diffraction patterns of **1**, **2** and **3**, unit cell measurements at different temperatures and structural views of **1**

$[Fe^{II}(TPMA)(en)](ClO_4)_2$ **(1)**, $[Fe^{II}(TPMA)(2\text{-pic})](ClO_4)_2$ (**2**) and $[Fe^{II}(TPMA)(pn)](ClO_4)_2$ **(3)** were synthesized by reacting $Fe(ClO_4)_2 \cdot xH_2O$ with the corresponding bidentate ligand in a 1:1 ratio followed by the addition of one equivalent of TPMA in methanol or methanol/ethanol mixtures. The resulting solution was stirred vigorously and then quickly filtered. Crystals of the three compounds were obtained by leaving the filtrate undisturbed overnight. The crystallization was performed under inert atmosphere in a glove box to avoid oxidation. **3** could not be obtained as single crystals of enough quality to solve the structure, but single crystal unit cell measurement and powder X-ray diffraction pattern indicate that it is isostructural to **1** (Fig. S1 in the ESI†).[9]

Structure of 1.

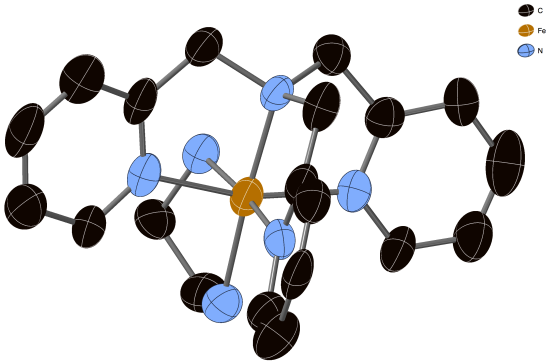

Fig. 1 Structure of $[Fe^{II}(TPMA)(en)]^{2+}$ complex in **1** at 120 K (C (black), N(blue), and Fe(brown). Hydrogen atoms have been omitted for clarity.

The crystal structure of $[Fe^{II}(TPMA)(en)](ClO_4)_2$ was solved by single crystal X-ray diffraction at 120 K. It crystallizes in the non-centrosymmetric orthorhombic *Pnn*2 space group (see Table 1). The asymmetric unit contains one crystallographically independent $[Fe^{II}(TPMA)(en)]^{2+}$ complex and two ClO_4^- anions. $[Fe^{II}(TPMA)(en)]^{2+}$ and one of the two ClO_4^- anions present a disorder. This disorder was modelled with two possible configurations of the Fe(II) complex with occupancies of 0.85 and 0.15. In both configurations, Iron(II) is coordinated by the four N of tetradentate TPMA and the two N from ethylenediamine leading to a distorted octahedral geometry (see Figs. 1 and 2 and S2 in the ESI†). The Fe-N bond lengths in the complex with a 0.85 occupancy lie in the range 1.970(14)-2.033(13) Å, which are similar to those of other TPMA Fe(II) complexes in the LS state.[5] This is in agreement with magnetic properties (see below). $[Fe^{II}(TPMA)(en)]^{2+}$ complexes present three CH···π contacts with two neighbouring ones involving two pyridine rings of TPMA and one ethylenediamine leading to a three dimensional structure with holes filled with ClO_4^- counteranions, which present numerous short contacts with $[Fe^{II}(TPMA)(en)]^{2+}$ complexes. It was not possible to solve the structure by single crystal X-ray diffraction at higher temperatures (300 and 360 K) due to the small size of the crystals and the increase of the disorder. Powder X-ray diffraction pattern of crystals of this compound at 300 K is consistent with the simulated one from the single crystal X-ray diffraction structure at 120 K (see Fig. S1 in the ESI†).

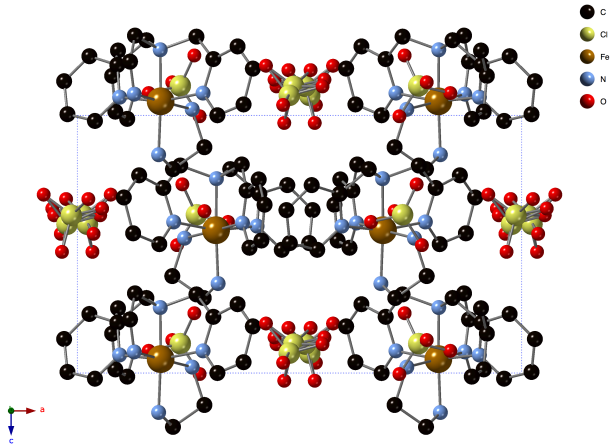

Fig. 2 Projection in the *ac* plane of the structure of **1** at 120 K (C(black), N(blue), O(red), Cl(yellow) and Fe(brown)). One of the two possible configurations of $[Fe^{II}(TPMA)(en)]^{2+}$ and hydrogen atoms have been omitted for clarity.

Structure of 2.

$[Fe^{II}(TPMA)(2\text{-pic})](ClO_4)_2$ crystallizes in the tetragonal chiral space groups $P4_1$ or $P4_3$ (see Table 1). The crystal structure at 90 K was solved in a crystal crystallizing in $P4_1$, while those at 120, 220 and 300 K were solved in crystals crystallizing in $P4_3$. Therefore, two enantiomorphs are found in **2**, in which the two space groups themselves constitute an enantiomeric pair. The asymmetric unit contains one crystallographically independent $[Fe^{II}(TPMA)(2\text{-pic})]^{2+}$ complex and two ClO_4^- anions. The Fe(II) ion of the complex is coordinated by the four N of tetradentate TPMA and the two N from 2-pic leading to a distorted octahedral geometry (see Figs. 3 and 4). The pyridine group from 2-pic is in trans to one of the pyridine rings of TPMA to minimize the steric repulsions. The Fe-N bond lengths lie in the range 1.992(3)-2.049(4) Å at 90 K, 2.058(3)-2.108(4) Å at 120 K, 2.166(4)-2.229(4) Å at 220 K and 2.174(5)-2.236(5) Å at 300 K. Distances at 90 K and 220 K are typical from the LS and HS state, respectively, similar to those of other TPMA Fe(II) complexes.[5] This indicates that from 90 to 220 K there is a complete spin transition in agreement with magnetic and Mössbauer measurements (see below). The changes in the unit cell with the temperature measured by single crystal X-ray diffraction in the same crystal are consistent with this spin transition as unit cell parameters increase more abruptly in this temperature range (see Fig. S3 in the ESI†). Most of the intermolecular interactions of the complex involve the perchlorate anions. The neighboring complexes do not present hydrogen bonds or π-π stacking interactions. Thus, $[Fe^{II}(TPMA)(2\text{-pic})]^{2+}$ complexes presents two CH···π contacts between pyridine rings of TPMA from neighboring complexes and two CH···π contacts involving a pyridine ring of TPMA and a pyridine ring of 2-pic from a neighboring complex at 90 K. This changes at 220 and 300 K. At these temperatures, $[Fe^{II}(TPMA)(2\text{-pic})]^{2+}$ complexes present two CH···CH short contacts involving a TPMA arm and a 2-pic ligand from different complexes. Therefore, as in **1,** the packing of the

$[Fe^{II}(TPMA)(2\text{-pic})]^{2+}$ complexes in the crystal structure of **2** is quite loose, as the cationic species are intercalated with the ClO_4^- counterions and lack strong intermolecular cation–cation interactions. The complexes form helices running along the *c* axis related by a 4-fold screw axis. They present opposite helicity in the crystals solved as $P4_1$ or $P4_3$ (see Fig. S4 in the ESI†). Powder X-ray diffraction pattern of crystals of this compound is consistent with the simulated one from the single crystal X-ray diffraction structure (see Fig. S5 in the ESI†).

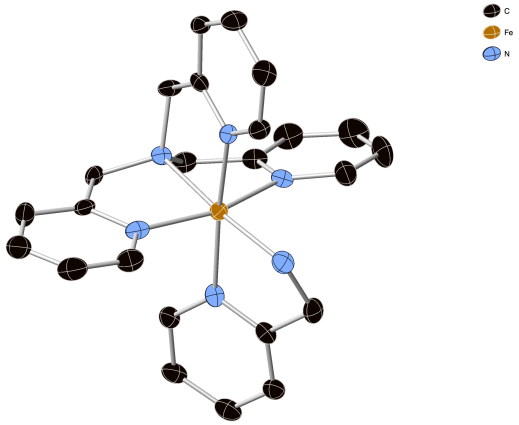

Fig. 3 Structure of $[Fe^{II}(TPMA)(2\text{-pic})]^{2+}$ complex in **2** at 90 K (C (black), N(blue), and Fe(brown). Hydrogen atoms have been omitted for clarity.

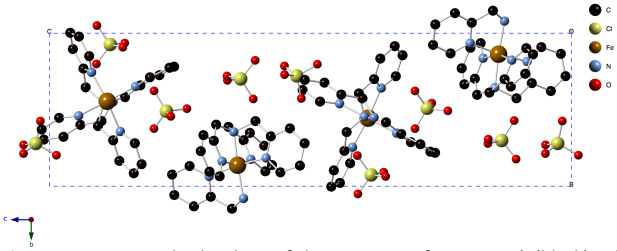

Fig. 4 Projection in the *bc* plane of the structure of **2** at 90 K (C(black), N(blue), O(red), Cl(yellow) and Fe(brown)). Hydrogen atoms omitted for clarity.

Magnetic properties.

The product of the molar magnetic susceptibility times the temperature ($\chi_M T$) of the three compounds is shown in Fig. 5. They present the same behavior in the heating and cooling modes in agreement with the lack of solvent molecules in the structures. Furthermore, the absence of strong intermolecular interactions leads to very gradual spin transitions. $\chi_M T$ of **2** shows an almost constant value of 3.6-3.7 $cm^3 \cdot K \cdot mol^{-1}$ in the temperature range 200-300 K, which corresponds to 100% Fe(II) with HS configuration (*S*=2). At lower temperatures, $\chi_M T$ shows a gradual decrease to reach a value close to 0, typical for a diamagnetic LS configuration, at 65 K (0.1 $cm^3 \cdot K \cdot mol^{-1}$). Therefore, from 200 to 65 K, $[Fe^{II}(TPMA)(2\text{-pic})](ClO_4)_2$ presents a complete and reversible spin transition. The $T_{1/2}$, defined as the temperature at which the HS and LS fractions are the same, is 131 K. These data are in agreement with the crystallographic measurements at 90 K, which show typical LS distances and consistent with Mössbauer data (see below). $\chi_M T$ of **1** shows a value of 3.3 $cm^3 \cdot K \cdot mol^{-1}$ at 400 K, close to the expected value for the HS state. At lower temperatures, there is a gradual decrease to reach a value close to zero at 170 K (0.3 $cm^3 \cdot K \cdot mol^{-1}$). **1** presents a complete and reversible spin-crossover at higher temperatures ($T_{1/2}$ = 290 K) than those of **2**. Again, the LS state below 200 K is consistent with structural data at 120 K and Mössbauer data (see below). $\chi_M T$ of **3** shows a gradual decrease from 3.4 $cm^3 \cdot K \cdot mol^{-1}$ at 400 K to a value close to zero below 210 K with a $T_{1/2}$ = 325 K.

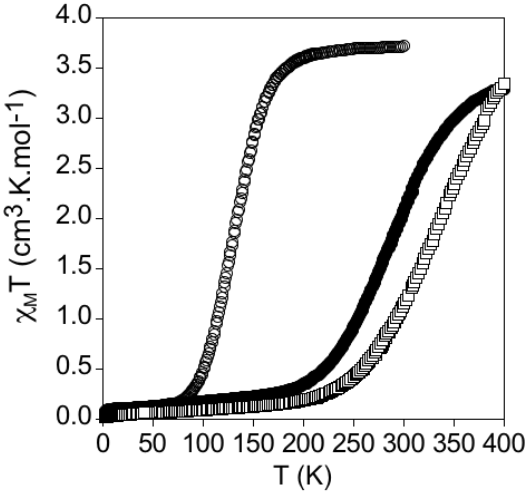

Fig. 5 Temperature dependence of the product of the molar magnetic susceptibility times the temperature ($\chi_M T$) of **1** (full circles), **2** (empty circles) and **3** (empty squares).

Photomagnetic properties.

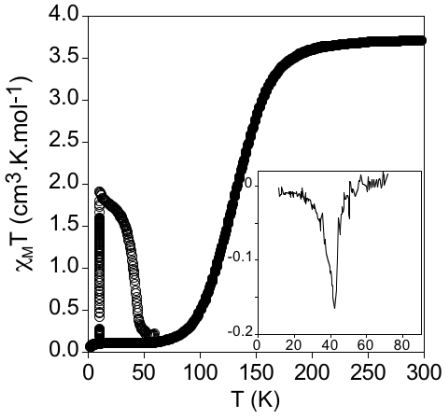

Fig. 6 Temperature dependence of the product of the molar magnetic susceptibility with temperature ($\chi_M T$) at 0.1 T for **2** before irradiation (filled circles) and after irradiation at 10 K and heating (empty circles). The inset graph shows the temperature dependence of the first derivative of $\chi_M T$ with respect to the temperature after irradiation.

1, **2** and **3** were irradiated with red (λ = 633 nm, optical power 12 mW cm^{-2}) and green light (λ = 532 nm, optical power 3.4 mW cm^{-2}) at 10 K in the SQUID. A drastic increase of the magnetic signal of **2** was observed after irradiation with red light. After about five hours, the irradiation was switched off. The temperature was then increased at a rate of 0.3 K min^{-1} and the magnetic susceptibility recorded. The $\chi_M T$ value after irradiation is higher than the value recorded in the dark at temperatures below 60 K (see empty circles in Fig. 6). The fraction of Fe(II) photoconverted after irradiation is calculated to be 50 %. This low photoconversion could be related to the strong absorption of the crystals, which results in the photoexcitation of the complexes close to the surface and not in the bulk. The LIESST temperature (T_{LIESST}), defined as the minimum of the derivate of $\chi_M T$ with temperature, is 43 K (see inset in Fig. 6). $T_{1/2}$ and T_{LIESST} values of **2** ($T_{1/2}$ = 131 K and T_{LIESST}= 43 K) are consistent with those previously obtained for other iron(II) complexes of TPMA showing LIESST effect such as $[Fe(TPMA)(xbim)](ClO_4)_2$ ($T_{1/2}$ = 196 on cooling and 203 K on heating and T_{LIESST} = 52 K) and $[Fe(TPMA)(xbim)](ClO_4)(TCNQ)_{1.5}\cdot DMF$ ($T_{1/2}$ = 145 K and T_{LIESST}= 50 K) (xbim = 1,1'-(α,α'-o-xylyl)-2,2'-bisimidazole and TCNQ = 7,7',8,8'-tetracyanoquinodimethane radical anion).[5,6,10] Previous studies have identified that these two values are related by the linear relationship, $T_{LIESST} = T_0 - 0.3\ T_{1/2}$.[11] T_0 has been proposed to be equal to 100, 120, 150, 180 and 200 K for monodentate, bidentate, tridentate, macrocyclic ligands and Prussian Blue analogs, respectively. In the case of TPMA compounds T_0 seems to be close to 100 K. This is consistent with the fact that LIESST effect could not be detected in **1** and **3** as their high $T_{1/2}$ values (290 K for **1** and 325 K for **3**) would lead to a too low T_{LIESST} to be detected (lower than 15 K). The high $T_{1/2}$ values of these compounds make the intersystem crossing processes too fast even at low temperatures to allow for a metastable state. More studies needed to understand the photomagnetic behavior of **2** (structure and relaxation kinetics of the photoinduced metastable state) are in progress.

Mössbauer spectroscopy.

The Mössbauer spectrum of **2** at 4 K (Figure 7b) consists of a single quadrupole doublet with narrow peaks. Estimated isomer shift relative to metallic αFe at 295 K, IS ~0.53 mm/s, and quadrupole splitting, QS ~ 0.45 mm/s (Table 2), are consistent with LS Fe(II).[5,12,13] At 220 K and above the spectra of **2** also show a single quadrupole doublet but the IS ~1.00 mm/s, 0.95 mm/s and QS~2.37 mm/s, 2.11 mm/s at 220 K and 295 K respectively, are significantly higher than those of LS Fe(II), consistent with HS Fe(II).[5,12,13]

The two-peak pattern observed for sample **1** between 100 and 200 K is asymmetric. This is often indication of more than one Fe species as suggested in the present case by the presence of two configurations of $[Fe^{II}(TPMA)(en)]^{2+}$ complex, according to single crystal X-ray diffraction data. The spectra were therefore analysed considering two Fe doublets. The estimated IS ~0.50 - 0.53 mm/s (doublet 1) and 0.45-0.48 mm/s (doublet 2) at 100 and 200 K, respectively, as well as QS ~0.41 mm/s and ~0.55 mm/s (Table 2) are consistent with LS Fe^{II} values, as expected from magnetization data. The doublet with estimated relative area ~15% may be attributed to the configuration of $[Fe^{II}(TPMA)(en)]^{2+}$ complex with a 0.15 occupancy calculated from crystallographic data (see above). Furthermore this doublet has higher QS as expected considering that the Fe sites are more distorted in this configuration.

The spectra of **2** taken in the temperature range 80 - 150 K show the presence of both HS and LS Fe(II), the relative areas of the HS doublet increasing with temperature. The increase of the IS values of both LS and HS doublets with decreasing temperature is a result of the second order Doppler shift. The QS of LS Fe(II) is only due to the asymmetry of the electric charges distribution in the lattice since no electric field gradient is created by the electrons in a ^1A_l electronic configuration. On the other hand a large electric field gradient is created by the electrons in the $^5T_2$ configuration of the HS Fe(II) thus explaining the higher QS observed for the HS state. The temperature dependence of the quadrupole splitting of the HS Fe(II) is due to the population of the excited electronic states.[5,13] Mössbauer data of **2** is fully consistent with the spin crossover transition observed in the temperature dependence of $\chi_M T$ (Fig. 5).

In the case of **1**, broadening of the doublet peaks occurs and an additional absorption band is observed at 250 K. This additional absorption band may be approximated by two quadrupole doublets with similar IS ~0.75 mm/s and different QS ~1.2 mm/s and ~2.1 mm/s (Table 2), both consistent with HS Fe(II). The similar IS of both HS Fe(II) is in agreement with identical coordination numbers as observed in single crystal X-ray diffraction data. The doublet with the highest QS is related to HS Fe(II) in the configuration with a 0.15 occupanccy, as it presents a more distorted octahedral environment. The relative areas of the HS Fe(II) species increase at the expense of the corresponding LS Fe(II) species in agreement with the increase in magnetization observed as the temperature increases above 200 K.

The absorption peaks at 250 K and above are significantly broadened. This broadening is hardly explained by oxidation of the compound since it increases with temperature and, moreover, spectra of two different samples at 100 K, performed both after and before measurements at room temperature, are identical within experimental error. The broadening may rather be explained by relaxation effects. When the frequency of the LS to the HS state interconversion ν_i is low compared to the frequencies related to the electric hyperfine interactions, ω_{hf}, two sharp distinct doublets are observed as in the case of **2**.[5,14,15] If ν_i and ω_{hf} are comparable, line broadening and coalescence of the lines occurs.[14,15] The absorption peaks of **1** at 250 K and above are broader than below 200 K most probably because ν_i is only slightly lower than ω_{hf}. The peak widths keep increasing with temperature as ν_i also increases becoming similar to ω_{hf} at 295 K.

The Mössbauer effect results of compound **1** clearly show that at 200 K and below all the Fe(II) is in the LS state in the two configurations of the complex. At 250 K and above a fraction of Fe(II) is in the HS state. Transition from LS to HS occurs in both

configurations of the complex. In agreement with the gradual spin crossover transition observed in the temperature dependence of $\chi_M T$ (Figure 5), the total fraction of Fe(II) in the HS state gradually increases with temperature above 250 K (Table 2) and the spin crossover transition is not yet complete at 295 K.

Conclusions

Three new mononuclear Fe(II) SCO complexes have been prepared and characterized by the combination of TPMA and three neutral bidentate ligands (pn, en and 2-pic). Structural and magnetic characterization demonstrates that they present a SCO behavior as reported in the literature for Fe(II) complexes of TPMA and bulkier bisimidazole bidentate ligands. Hence, TPMA has been confirmed as an effective ligand platform for achieving temperature and light driven SCO with a variety of bidentate ligands. The following conclusions can be extracted from this work: i) The use of ligands such as en, pn and 2-pic enables tuning the $T_{1/2}$ from 130 to 325 K; ii) LIESST effect is only observed in this family of complexes for compounds showing relatively low $T_{1/2}$ (below 200 K); iii) The absence of strong intermolecular interactions and solvent molecules leads in the three compounds to reversible and gradual spin transitions.

Therefore, the use of small neutral bidentate ligands and TPMA coordinated to Fe(II) is a simple strategy to obtain SCO in a wide range of temperatures. Interestingly, these relatively small bidentate ligands favour the crystallization in non-centrosymmetric space groups in contrast to bulkier bisimidazole and derivatives bidentate ligands. This could open the way to other phenomena in coexistence with the SCO such as ferroelectricity, which has been recently reported for a salt of the well-known iron(II) spin crossover complex $[Fe(3\text{-}bpp)_2]^{2+}$ (3-bpp = 2,6-bis(pyrazol-3-yl)pyridine).[16] An interesting possibility in this context is replacement of racemic pn ligand in **3** by the chiral ligands (*S*)-1,2-diaminopropane or (*R*)-1,2-diaminopropane. The preparation of these compounds and the study of these properties are in progress.

Experimental

Synthetic procedures.

Caution: The perchlorate salts of metal complexes with organic ligands are potentially explosive. Only small quantities of the compound should be prepared and handled with much care!

Synthesis of $[Fe(TPMA)(en)](ClO_4)_2$ (1). A solution of $Fe(ClO_4)_2 \cdot xH_2O$ (72.6 mg, 0.2 mmol) in methanol (2 mL) was added to a solution of ethylenediamine (12.02 mg, 0.2 mmol) in ethanol (8 mL) with stirring. The yellowish solution obtained was stirred for ca. 30 seconds, followed by addition of a solution of tris(2-pyridylmethyl)amine (58 mg, 0.2 mmol) in methanol (2 mL). The dark-red solution obtained was stirred vigorously for a few seconds and then quickly filtered. The filtrate was left undisturbed under inert atmosphere overnight. Block-shaped yellow-brown crystals that formed were recovered by filtration and washed with ethanol and diethyl ether. The crystals obtained were suitable for X-ray diffraction. The composition, checked by microanalysis, shows a Fe:Cl ratio close to 1:2. $FeC_{20}H_{26}N_6O_8Cl_2$ (605.22): calcd. C 39.69, N 13.89, H 4.33; found C 39.25, N 13.81, H 4.24.

Synthesis of $[Fe(TPMA)(2\text{-}pic)](ClO_4)_2$ (2) A solution of $Fe(ClO_4)_2 \cdot xH_2O$ (72.6 mg, 0.2 mmol) in methanol (2 mL) was added to a solution of 2-picolylamine (21.63 mg, 0.2 mmol) in methanol (8 mL) with stirring. The colorless solution obtained was stirred for ca. 30 seconds, followed by addition of a solution of tris(2-pyridylmethyl)amine (58 mg, 0.2 mmol) in methanol (2 mL). The dark-red solution obtained was stirred vigorously for a few seconds and then quickly filtered. The filtrate was left undisturbed under inert atmosphere overnight. Block-shaped red crystals that formed were recovered by filtration and washed with ethanol and diethyl ether. The crystals obtained were suitable for X-ray diffraction. The composition, checked by microanalysis, shows a Fe:Cl ratio close to 1:2. $FeC_{24}H_{26}N_6O_8Cl_2$ (653.25): calcd. C 44.12, N 12.87, H 4.01; found C 44.20, N 12.93, H 3.90.

Synthesis of $[Fe(TPMA)(pn)](ClO_4)_2$ (3). A solution of $Fe(ClO_4)_2 \cdot xH_2O$ (72.6 mg, 0.2 mmol) in ethanol (2 mL) was added to a solution of 1,2-diaminopropane (14.82 mg, 0.2 mmol) in ethanol (8 mL) with stirring. The yellowish solution obtained was stirred for ca. 30 seconds, followed by addition of a solution of tris(2-pyridylmethyl)amine (58 mg, 0.2 mmol) in ethanol (2 mL). The dark-red solution obtained was stirred vigorously for a few seconds and then quickly filtered. The filtrate was left undisturbed under inert atmosphere overnight. The dark-red precipitate was recovered by filtration and washed with ethanol and diethyl ether. The composition, checked by microanalysis, shows a Fe:Cl ratio close to 1:2. $FeC_{21}H_{28}N_6O_8Cl_2$ (619.23): calcd. C 40.73, N 13.57, H 4.56; found C 39.98, N 13.39, H 4.47.

Crystallography.

Single crystals of all the complexes were mounted on a glass fiber using a viscous hydrocarbon oil to coat the crystal and then transferred directly to the cold nitrogen stream for data collection. X-ray data were collected at 90, 120, 220 and 300 K for **2** and at 120 K for **1** on a Supernova diffractometer equipped with a graphite-monochromated Enhance (Mo) X-ray Source (λ = 0.71073 Å). The program CrysAlisPro, Oxford Diffraction Ltd., was used for unit cell determinations and data reduction. Empirical absorption correction was performed using spherical harmonics, implemented in the SCALE3 ABSPACK scaling algorithm. Crystal structure of **2** was solved by direct methods with the SIR97 program,[17] and refined against all F^2 values with the SHELXL-2013 program,[18] using the WinGX graphical user interface.[19] The structure of **1** was solved with the ShelXT structure solution program[20] and refined with the SHELXL-2013 program,[18] using Olex2.[21] The Flack's absolute parameter (x) was used to determine the space group of the crystals of **2**. They exhibit a x parameter close to 0. This parameter lies within the range that indicates that the absolute structure is valid and that they are

enantiopure.[22] Although the crystal of **1** is chiral, a twin component was found with ratios 0.91:0.09. Non-hydrogen atoms were refined anisotropically (except as noted) and hydrogen atoms were placed in calculated positions refined using idealized geometries (riding model) and assigned fixed isotropic displacement parameters. The use of restraints in the refinement of the structures is documented in the corresponding CIFs. Data collection and refinement statistics are collected in Table 1. CCDC-1828113 to 1828117 contain the supplementary crystallographic data for this paper. These data can be obtained free of charge from The Cambridge Crystallographic Data Centre via www.ccdc.cam.ac.uk/data_request/cif. For X-Ray powder pattern, a 0.5 mm glass capillary was filled with a polycrystalline sample of de complexes and mounted and aligned on an Empyrean PANalytical powder diffractometer, using CuKα radiation (λ = 1.54177 Å). A total of 3 scans were collected at room temperature in the 2θ range 5-40º.

Physical characterization.

The Fe/Cl ratios were measured with a Philips ESEM X230 scanning electron microscope equipped with an EDAX DX-4 microsonde. Elemental analyses (C, H, and N) were performed with a CE Instruments EA 1110 CHNS Elemental analyzer. Magnetic measurements were performed with a Quantum Design MPMS-XL-5 SQUID magnetometer in the 2 to 400 K temperature range with an applied magnetic field of 0.1 T at a scan rate of 1 K/min on a polycrystalline sample. Photomagnetic measurements were performed irradiating with a 30993 cylindrical Helium-Neon Laser system from Research Electro-Optics and a Diode Pumped Solid State Laser DPSS-532-20 from Chylas and a coupled via an optical fiber to the cavity of the SQUID magnetometer. The optical power at the sample surface was adjusted to 12 and 3.4 $mW \cdot cm^{-2}$, and it was verified that it resulted in no significant change in magnetic response due to heating of the sample. The photomagnetic samples consisted of a thin layer of compound whose weight was corrected by comparison of a thermal spin crossover curve with that of a more accurately weighted sample of the same compound. Mössbauer spectra of **1** and **2** were collected between 298 and 4 K in transmission mode using a conventional constant-acceleration spectrometer and a 25 mCi ^{57}Co source in a Rh matrix. The velocity scale was calibrated using α-Fe foil. Isomer shifts, IS, are given relative to this standard at room temperature. The absorbers were obtained by gently packing the sample into perspex holders. Absorber thicknesses were calculated on the basis of the corresponding electronic mass-absorption coefficients for the 14.4 keV radiation, according to Long *et al.*[23] Low-temperature measurements were performed in a bath cryostat with the sample immersed in liquid He at 4 K and He or N_2 exchange gas above 4 K. The spectra were fitted to Lorentzian lines using a non-linear least-squares method.[24]

Conflicts of interest

There are no conflicts to declare".

Acknowledgements

Financial support from the EU (ERC Advanced Grant SPINMOL), the Spanish MINECO (CTQ2014-52758-P, MAT-2014-56143-R, MAT2017-89993-R and Unidad de Excelencia María de Maeztu MDM-2015-0538), the Generalitat Valenciana (Prometeo) is gratefully acknowledged. C2TN/IST authors gratefully acknowledge the FCT support through the UID/Multi/04349/2013 project. We thank J. M. Martínez-Agudo and G. Agustí from the Universidad de Valencia for the magnetic measurements.

Notes and references

1 See for general reviews: Eds. P. Gütlich and H.A. Goodwin, Spin Crossover in Transition Metal Compounds, *Topics in Current Chemistry*, Springer Verlag, Berlin-Heidelberg-New York, 2004, vols. *233-235*. Ed. M. A. Halcrow, Spin-Crossover Materials: Properties and Applications, John Wiley & Sons, Chichester, UK, 2013.

2 (a) O. Kahn and C. Jay Martinez, *Science* 1998, **279**, 44; (b) J. F. Létard, P. Guionneau and L. Goux-Capes, *Top. Curr. Chem.* 2004, **235**, 221; (c) T. Mahfoud, G. Molnar, S. Cobo, L. Salmon, C. Thibault, C. Vieu, P. Demont and A. Bousseksou, *Appl. Phys. Lett.,* 2011, **99,** No. 053307; (d) N. Baadji and S. Sanvito, S. *Phys. Rev. Lett.,* 2012, **108,** 217201; (e) I. R. Jeon, J. G. Park, C. R. Haney and T. D. Harris, *Chem. Sci.,* 2014, **5**, 2461; (f) J. Dugay, M. Giménez-Marqués, T. Kozlova, H. W. Zandbergen, E. Coronado and H. S. J. van der Zant, *Adv. Mater.,* 2015, **27**, 1288.

3 K. Senthil Kumar and M. Ruben, Coord. Chem. Rev., 2017, 346, 176.

4 (a) H. Toftlund, *Coord. Chem. Rev.,* 1989, **94**, 67; (b) B. Li, R. J. Wei, J. Tao, R. B. Huang, L. S. Zheng and Z. Zheng, *J. Am. Chem. Soc.,* 2010, **132**, 1558.

5 H. V. Phan, P. Chakraborty, M. Chen, Y. M. Calm, K.Kovnir, L. K. Keniley, Jr., J. M. Hoyt, E. S. Knowles, C. Besnard, M. W. Meisel, A. Hauser, C. Achim and M. Shatruk, *Chem. Eur. J.*, 2012, **18**, 15805.

6 H. Phan, S. M. Benjamin, E. Steven, J. S. Brooks and M. Shatruk, *Angew. Chem. Int. Ed.,* 2015, **54**, 823.

7 (a) K. S. Min, A. DiPasquale, A. L. Rheingold and J. S. Miller, *Inorg. Chem.,* 2007, **46**, 1048; (b) J. G. Park, I. R. Jeon and T. D. Harris, *Inorg. Chem.,* 2015, **54**, 359; (c) E. Milin, S. Belaïd, V. Patinec, S. Triki, G. Chastanet and M. Marchivie, *Inorg. Chem.,* 2016, **55**, 9038; (d) M. van der Meer, Y. Rechkemmer, F. D. Breitgoff, R. Marx, P. Neugebauer, U. Frank, J. van Slageren and B. Sarkar, *Inorg. Chem.,* 2016, **55**, 11944.

8 (a) M. Nihei, M. Ui, M. Yokota, L. Han, A. Maeda, H. Kishida, H. Okamoto and H. Oshio, *Angew. Chem. Int. Ed.,* 2005, **44**, 6484; (b) R. J. Wei, Q. Huo, T. Tao, R. B. Huang and L. S. Zheng, *Angew. Chem. Int. Ed.,* 2011, **50**, 8940.

9 Single crystal X-ray diffraction unit cell measurents at 120 K of **3**. a = 9.914(4) Å, b = 15.910(2) Å and c = 17.0157(18) Å, V = 2648(1) $Å^3$. Unit cell calculated from 536 reflections.

10 These compounds were irradiated at 5 K. $[Fe(TPMA)(xbim)](ClO_4)_2$ was warmed at 0.5 K min^{-1} after irradiation. This could prevent comparison of T_{LIESST} with that of the other two compouns warmed at 0.3 K min^{-1}.

11 (a) J. F. Létard, P. Guionneau, O. Nguyen, J. Sanchez Costa, S. Marcen, G. Chastanet, M. Marchivie and L. Goux-Capes,

Chem. Eur. J., 2005, **11**, 4582 ; (b) J. F. Létard, *J. Mater. Chem.,* 2006, **16**, 2550.
12 P. Gütlich, Y. Garcia and H. A. Goodwin, *Chem. Soc. Rev.,* 2000, **29**, 419.
13 N. N. Greenwood, T. C. Gibb, Mössbauer Spectroscopy, Chapman and Hall, Ltd. Publishers, London, 1971.
14 H. Ohshio, Y. Maeda and Y. Takashima, *Inorg. Chem.,* 1983, **22**, 2684.
15 P. Adler, H. Spiering and P. Gütlich, *Inorg. Chem.,* 1987, **26**, 3840.
16 V. Jornet-Mollá. Y. Duan, C. Giménez-Saiz, Y. Y. Tang, P. F. Li, F. M. Romero and R. G. Xiong, *Angew. Chem. Int. Ed.,* 2017, **56**, 14052.
17 A. Altomare, M. C. Burla, M. Camalli, G. L. Cascarano, C. Giacovazzo, A. Guagliardi, A. G. G. Moliterni, G. Polidori and R. Spagna, *J. Appl. Cryst*., 1999, **32**, 115.
18 G. M. Sheldrick, *Acta Cryst.,* 2015, **C71,** 3.
19 L. J. Farrugia, *J. Appl. Cryst.,* 2012, **45**, 849.
20 G. M. Sheldrick, *Acta Cryst.,* 2015, **A71,** 3.
21 O. V. Dolomanov, L. J. Bourhis, R. J. Gildea, J. A. K. Howard, H. Puschmann, *J. Appl. Cryst.* 2009, **42**, 339.
22 H. D. Flack and G. Bernardinelli, *J. Appl. Crystallogr.,* 2000, **33**, 1143.
23 G. J. Long, T. E.Cranshaw and G. Longworth, *Mossb. Effect. Ref. Data J.*, 1983, **6**, 42.
24 J.C. Waerenborgh, P. Salamakha, O. Sologub, A.P. Gonçalves, C. Cardoso, S. Sério, M. Godinho and M. Almeida, *Chem. Mater.,* 2000, **12**, 1743.

Journal Name

ARTICLE

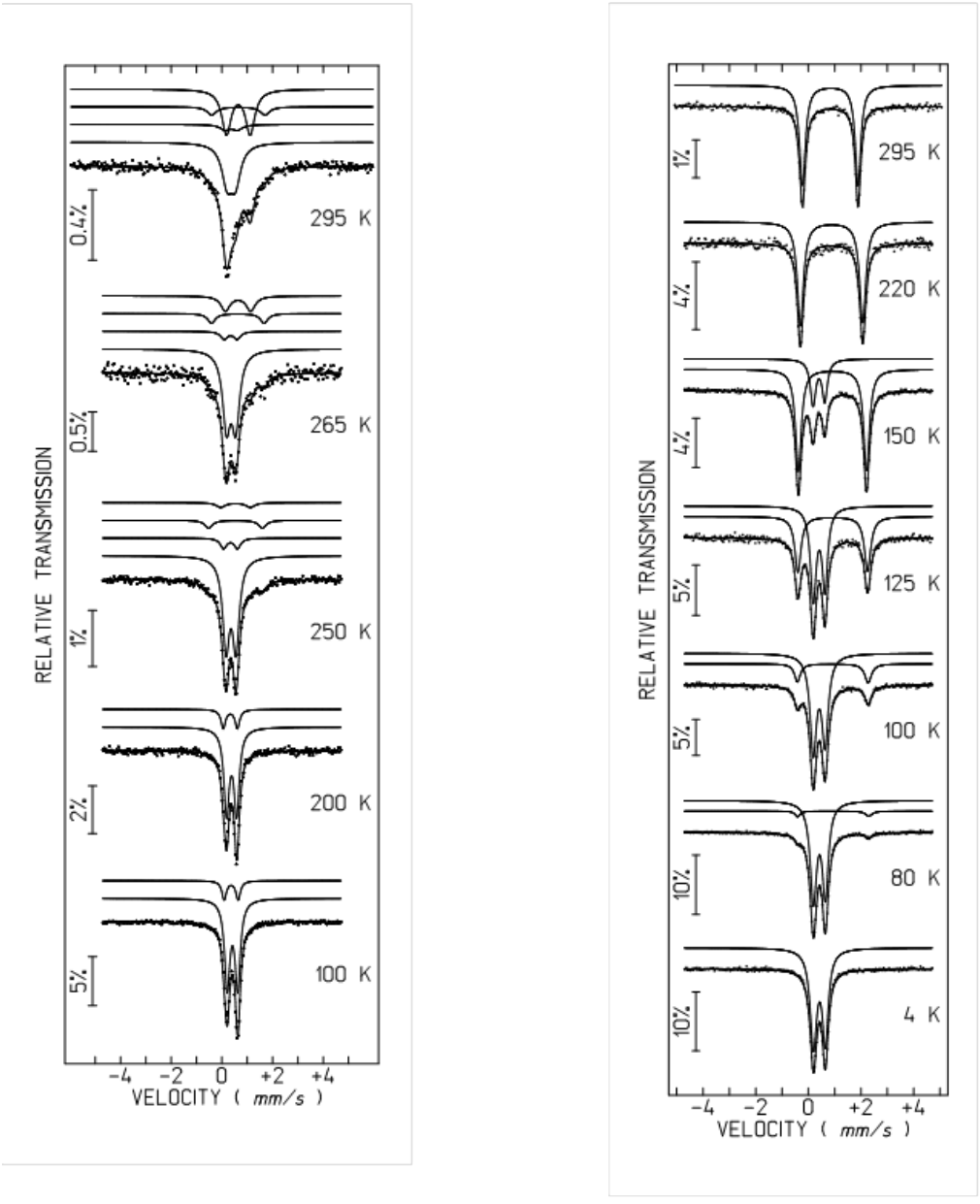

(a) (b)

Fig. 7 Mössbauer spectra of **1** (a) and **2** (b) taken at different temperatures.

Table 1. Crystallographic data for compounds **1** and **2**.

Compound	**1**	**2**	**2**	**2**	**2**
Empirical formula	$C_{20}H_{26}Cl_2FeN_6O_8$	$C_{24}H_{26}Cl_2FeN_6O_8$	$C_{24}H_{26}Cl_2FeN_6O_8$	$C_{24}H_{26}Cl_2FeN_6O_8$	$C_{24}H_{26}Cl_2FeN_6O_8$
Formula weight	605.22	653.26	653.26	653.26	653.26
Crystal colour	Red-brown	Red	Red	Red	Red
Crystal size (mm)	0.16x0.14x0.11	0.87x0.35x0.26	0.31x0.11x0.10	0.45x0.14x0.11	0.45x0.14x0.11
Temperature (K)	120(2)	90(2)	120(2)	220(2)	300(2)
Wavelength (Å)	0.71073	0.71073	0.71073	0.71073	0.71073
Crystal system	Orthorhombic	Tetragonal	Tetragonal	Tetragonal	Tetragonal
Space group	*P*nn2	$P4_1$	$P4_3$	$P4_3$	$P4_3$
a (Å)	16.9207(6)	9.25960(10)	9.28910(10)	9.36020(10	9.38270(10)
b (Å)	15.7742(6)	9.25960(10)	9.28910(10)	9.36020(10	9.38270(10)
c (Å)	9.8061(5)	31.6205(7)	31.9712(4)	32.5285(5)	32.7021(6)
V (Å^3)	2617.35(19)	2711.15(8)	2758.71(7)	2849.93(8)	2878.93(8)
ρ_{calc} (Mg/m^3)	1.536	1.600	1.573	1.523	1.507
$\mu(Mo_{K\alpha})$ (mm^{-1})	0.836	0.814	0.800	0.774	0.766
θ range (°)	3.433-27.496	3.887-27.216	3.353-27.494	3.319-27.477	3.305-27.478
Reflns collected	23100	10061	25242	16450	16751
Independent reflns (R_{int})	5990 (0.0739)	5400 (0.0249)	5859 (0.0259)	4907 (0.0346)	5942 (0.0418)
L. S. parameters, *p*/ restraints, *r*	410/54	370/1	370/1	370/1	370/1
Absolute structure parameter	0.13(8)	0.04(2)	0.014(5)	-0.015(8)	-0.019(12)
$R1(F)$,[a] $I > 2\sigma(I)$	0.0871	0.0368	0.0342	0.0441	0.0523
$wR2(F^2)$,[b] all data	0.2644	0.0761	0.0845	0.0973	0.1271
$S(F^2)$,[c] all data	1.039	1.051	1.072	1.008	1.008
Flack parameter	0.09(6)	0.04(2)	0.014(5)	-0.015(8)	-0.019(12)

[a] $R1(F) = \sum||F_O|-|F_C||/\sum|F_O|$; [b] $wR2(F^2) = [\sum w(F_O^2-F_C^2)^2/\sum wF_O^4]^{1/2}$; [c] $S(F^2) = [\sum w(F_O^2-F_C^2)^2/\sum n + r - p)]^{1/2}$

Table 2. Estimated parameters from the Mössbauer spectra of **1** and **2** at different temperatures.

Compound	T	IS	QS, ε	Γ	Fe^{II} spin	I
1	295 K	0.45	0.33	0.50	LS	42%
		0.45	0.49	0.47	LS*	5%
		0.73	2.10	0.44	HS*	9%
		0.73	0.94	0.44	HS	44%
	265 K	0.48	0.36	0.37	LS	69%
		0.46	0.51	0.33	LS*	6%
		0.75	2.08	0.37	HS*	9%
		0.76	1.00	0.43	HS	16%
	250 K	0.47	0.39	0.33	LS	78%
		0.45	0.55	0.31	LS*	8%
		0.75	2.12	0.37	HS*	8%
		0.75	1.17	0.42	HS	6%
	200 K	0.50	0.40	0.25	LS	84%
		0.45	0.56	0.21	LS*	16%
	150 K	0.51	0.41	0.26	LS	84%
		0.46	0.53	0.22	LS*	16%
	100 K	0.53	0.41	0.25	LS	85%
		0.48	0.55	0.21	LS*	15%
2	295 K	0.95	2.11	0.27	HS	100%
	220 K	1.00	2.37	0.28	HS	100%
	150 K	0.51	0.44	0.25	LS	28%
		1.02	2.59	0.27	HS	72%
	125 K	0.52	0.44	0.27	LS	58%
		1.04	2.65	0.28	HS	42%
	100 K	0.52	0.44	0.30	LS	83%
		1.04	2.69	0.27	HS	17%
	80 K	0.53	0.45	0.30	LS	94%
		1.06	2.68	0.22	HS	6%
	4 K	0.53	0.45	0.30	LS	100%

* Second configuration of $[Fe^{II}(TPMA)(en)]^{2+}$ complex in compound **1**. IS (mm/s) isomer shift relative to metallic α-Fe at 295 K; QS (mm/s) quadrupole splitting; Γ (mm/s) full width at half maximum; I relative area. Estimated errors ≤ 0.02 mm/s for IS, QS, Γ and <4% for I.